Electronic Supplementary Information

Tailoring Dual Cross-linked Polymer-Ionic Liquid Composites by Blending Co-crystallizable Polymers for Stretchable Electronics

Minjun Kim,† Moonsung Park,† Hobin Seon, Sohyun Choi, Hee Joong Kim,* Sangwon Kim*

Department of Polymer Science and Engineering & Program in

Environmental and Polymer Engineering, Inha University, Incheon 22212, Republic of Korea.

† These authors contributed equally.

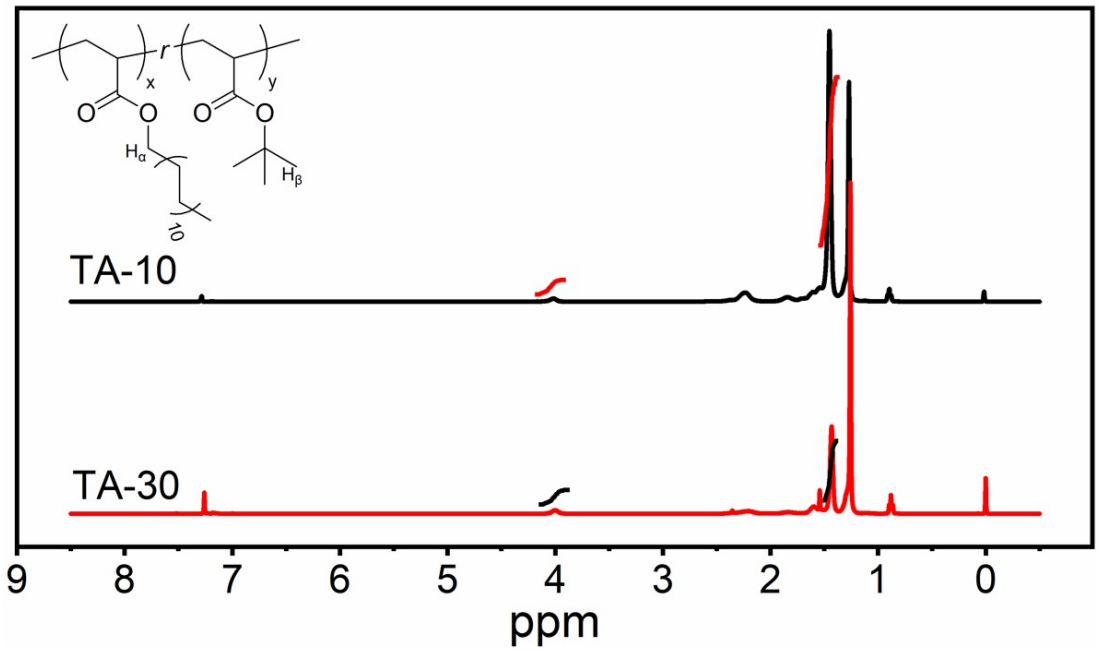

Fig. S1 ^{1}H-NMR spectra of the TA-10 (x:y = 9:91) and TA-30 (x:y = 28:72) copolymers (solvent: $CDCl_3$).

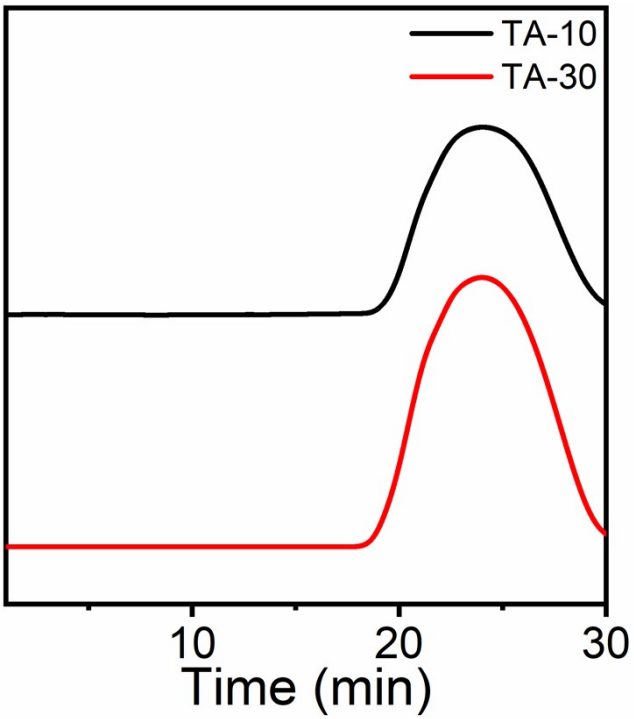

Fig. S2 SEC traces of TA-10 and TA-30 copolymers (THF mobile phase, 1 ml min^{-1} flow rate).

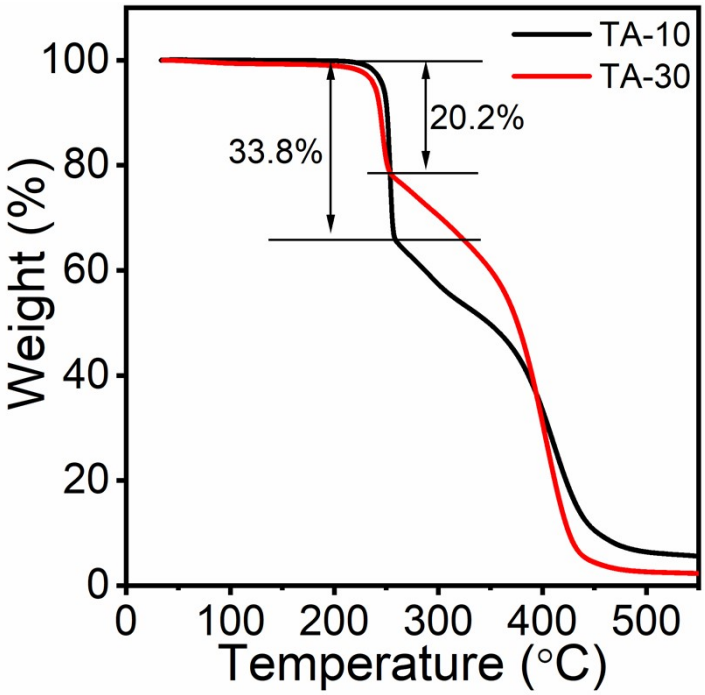

Fig. S3 TGA curves of the TA-10 and TA-30 copolymers (heating rate: 10 ˚C min^{-1}).

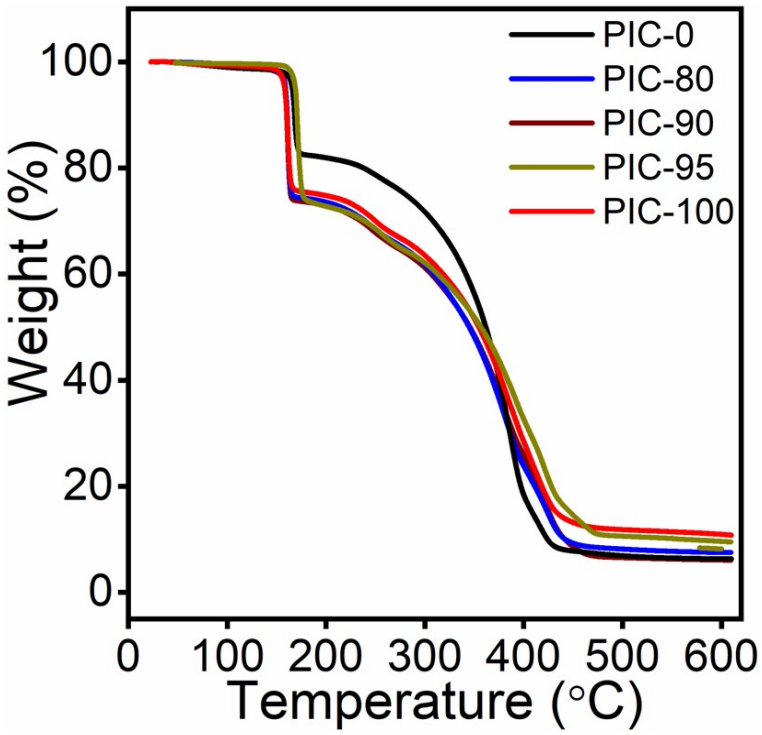

Fig. S4 TGA curves of PICs.

Based on the TGA results, the polymer-IL composites exhibit a precipitous drop near T = 175 °C. This prominent weight loss is associated with the elimination of the *tert*-butyl group via McLafferty rearrangement reaction.[1] The mole fraction of A22 in copolymers and content of ILs in the composites were calculated based on the degree of weight loss, assuming the reaction of all *t*BA monomers in composites at this temperature range.

1 S. Özlem and J. Hacaloglu, *J. Anal. Appl. Pyrolysis*, 2013, **104**, 161-169.

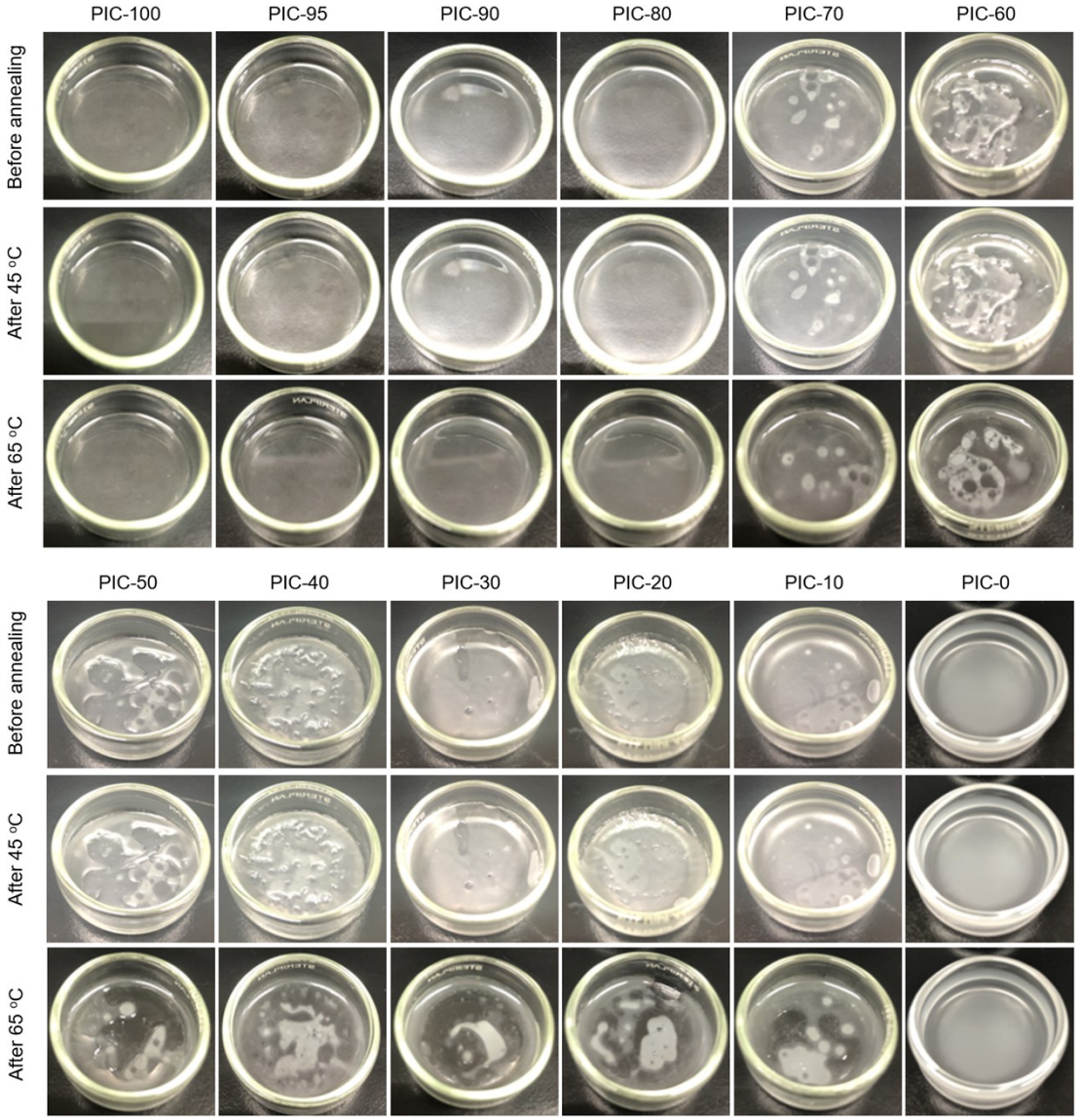

Fig. S5 Photographs of the composites before and after thermal annealing at 45 ˚C and 65 ˚C for 24 h.

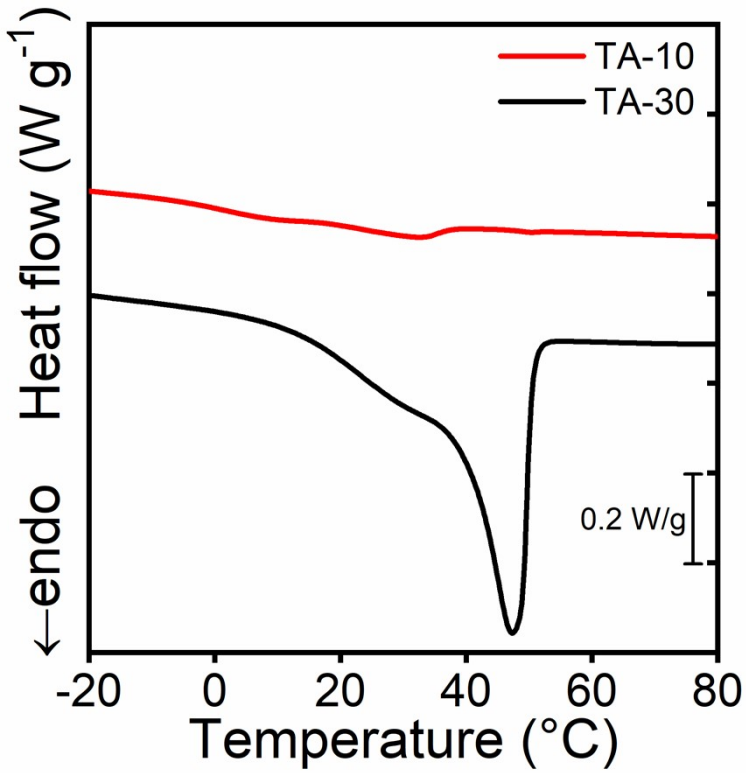

Fig. S6 DSC traces of the TA-10 and TA-30 copolymers obtained during the second heating process (heating rate: 10 ˚C min^{-1}). The degrees of crystallinity of the copolymers were 4.2% and 75.7% for TA-10 and TA-30, respectively.

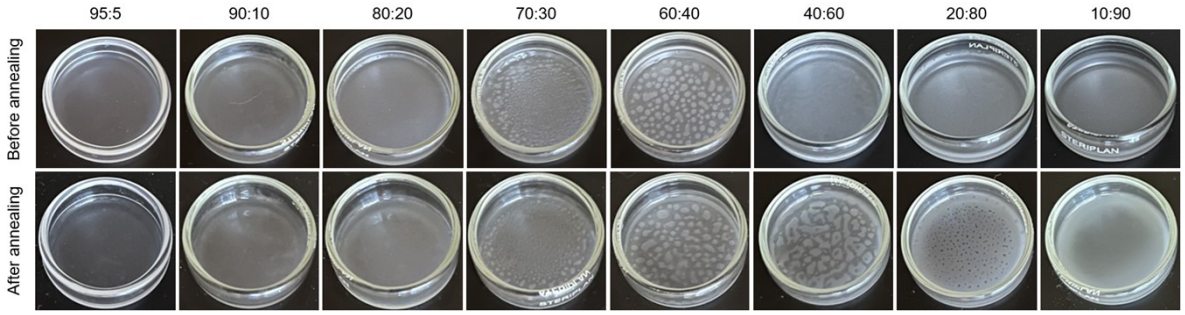

Fig. S7 Photographs of the TA-10:TA-30 (wt%) polymer blends before and after thermal annealing. As-prepared blend samples retain the state of the miscibility as they go through the thermal annealing process at 65 ˚C for 24 h.

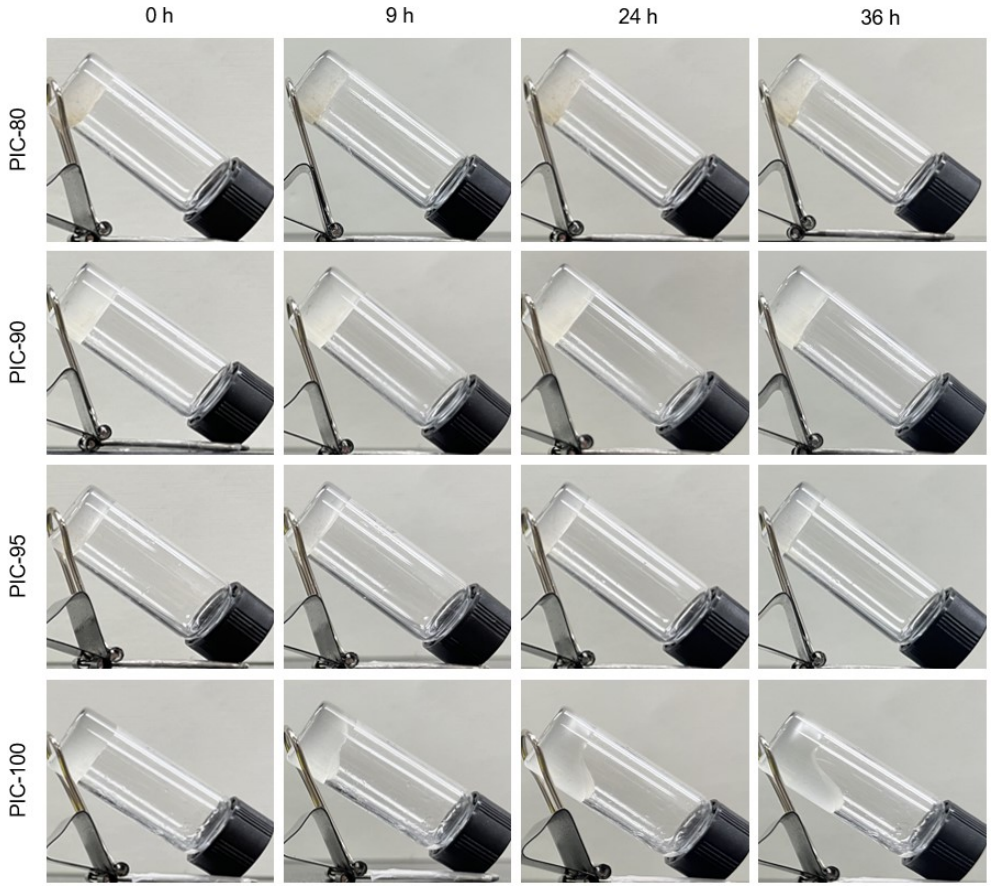

Fig. S8 Vial tilt test results for PICs. The tilted specimens were thermal annealed at 40 ˚C for 0, 9, 24, and 36 h.

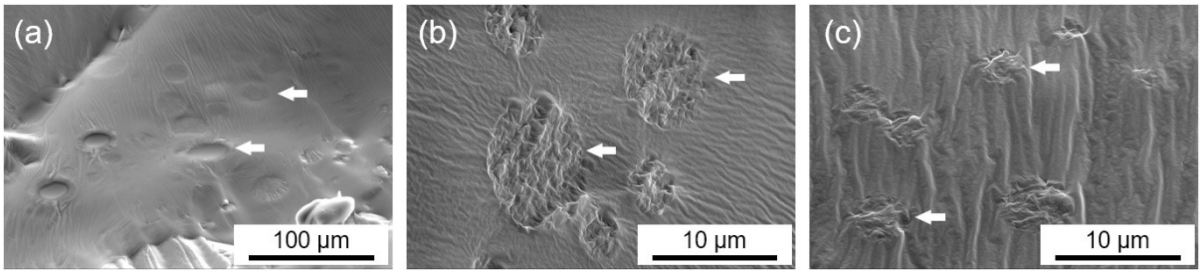

Fig. S9 Cross-sectional SEM images of (a) PIC-80, (b) PIC-90, and (c) PIC-95 (arrow indicates a crystalline domain).

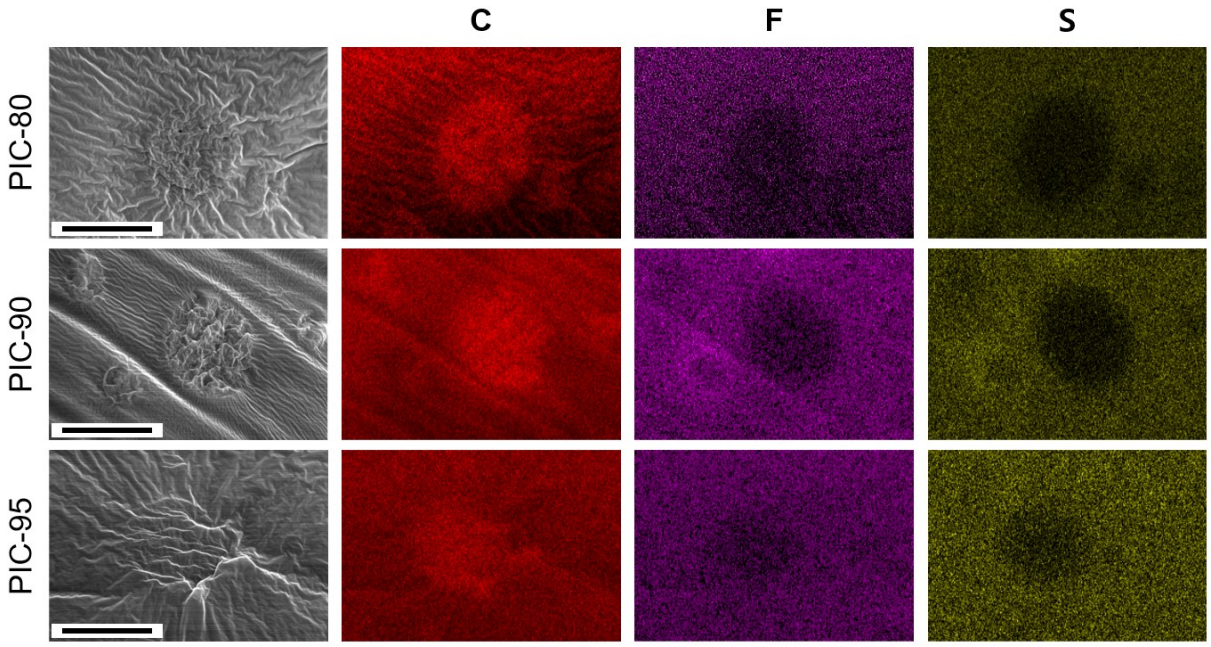

Fig. S10 SEM images and corresponding EDS mapping of C, F, and S elements of the PIC specimens. The scale bars correspond to 10 μm. The same brightness adjustment of images has been applied to the F elemental mapping for visualization.

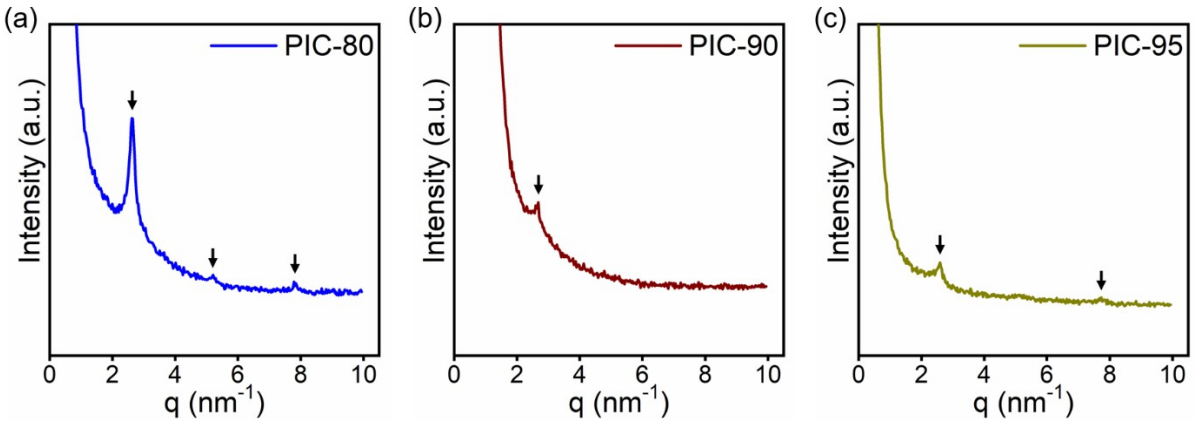

Fig. S11 SAXS profiles for PICs obtained at room temperature.

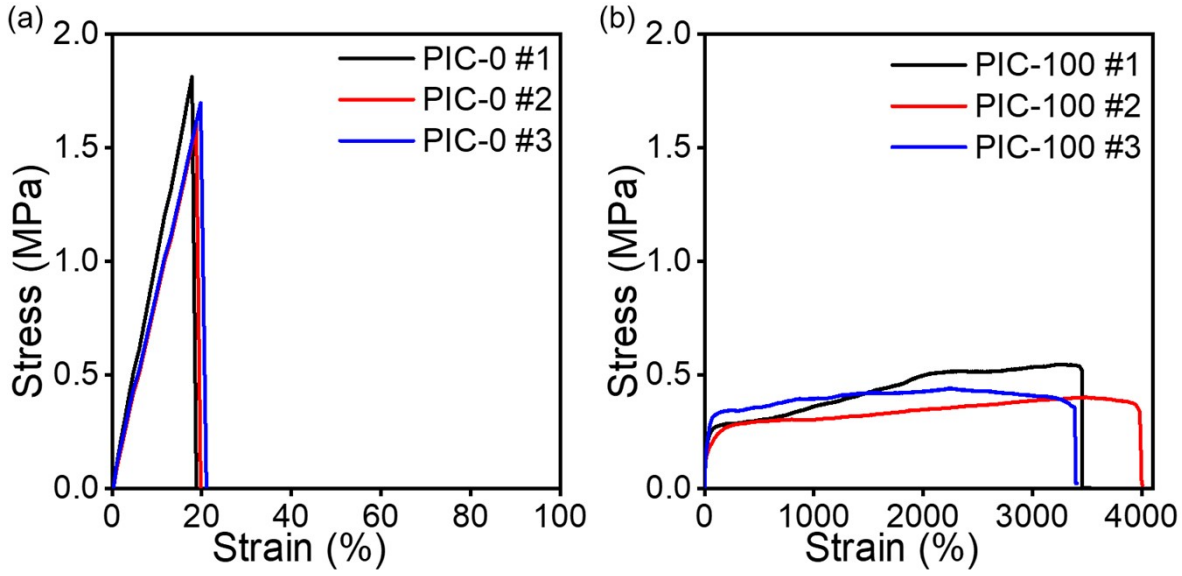

Fig. S12 Stress-strain curves of the pristine (a) PIC-0 and (b) PIC-100 specimens. Test were run in triplicate.

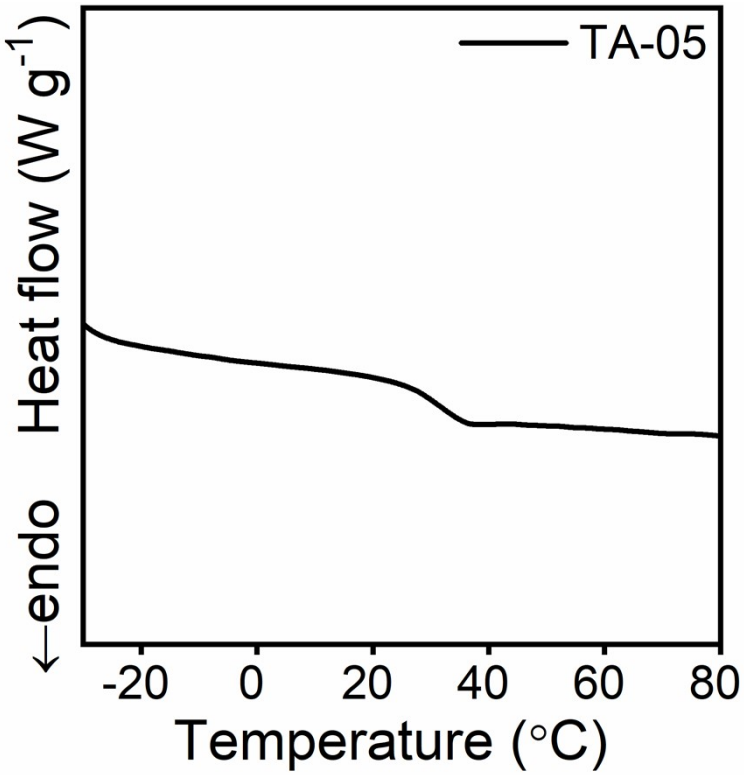

Fig. S13 DSC trace of TA-05 during the second heating cycle (heating rate: 10 ˚C min^{-1}).

Crystalline domains can shift the glass transition temperature (T_g) or even mask the glass transition, and this behavior sometimes makes the estimation of T_g difficult in semicrystalline polymers. TA copolymers with high A22 contents (>15 mol%) exhibit pronounced melting peaks in the DSC traces while the glass transition is not well identified, presumably due to the existence of crystalline regions. Therefore, the dynamics of the A22 segments in the copolymers was approximated via the DSC measurement of TA-05 (A22 = 5 mol%, *t*BA = 95 mol%). Fig. S13 shows that TA-05 is amorphous, devoid of crystallization. Based on T_g = 30.1 ˚C of TA-05, T_g associated with A22 (TA-100) was calculated using on the Fox equation ($T_{g\,A22}$ = −32.8 ˚C). T_g for TA-0 (P*t*BA) was assumed to be 43 ˚C in the calculation.

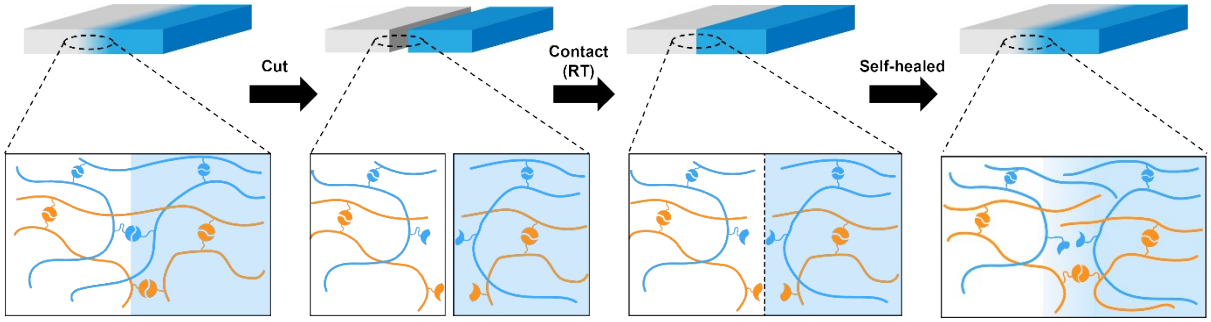

Fig. S14 Schematic illustration of the self-healing process conducted at room temperature. Cutting involves the preferential dissociation of cross-links at the interface. The cross-links formed through the association (orange) are reversible and can reform during self-healing. In contrast, limited mending occurs in crystallization (blue) below the melting temperature.

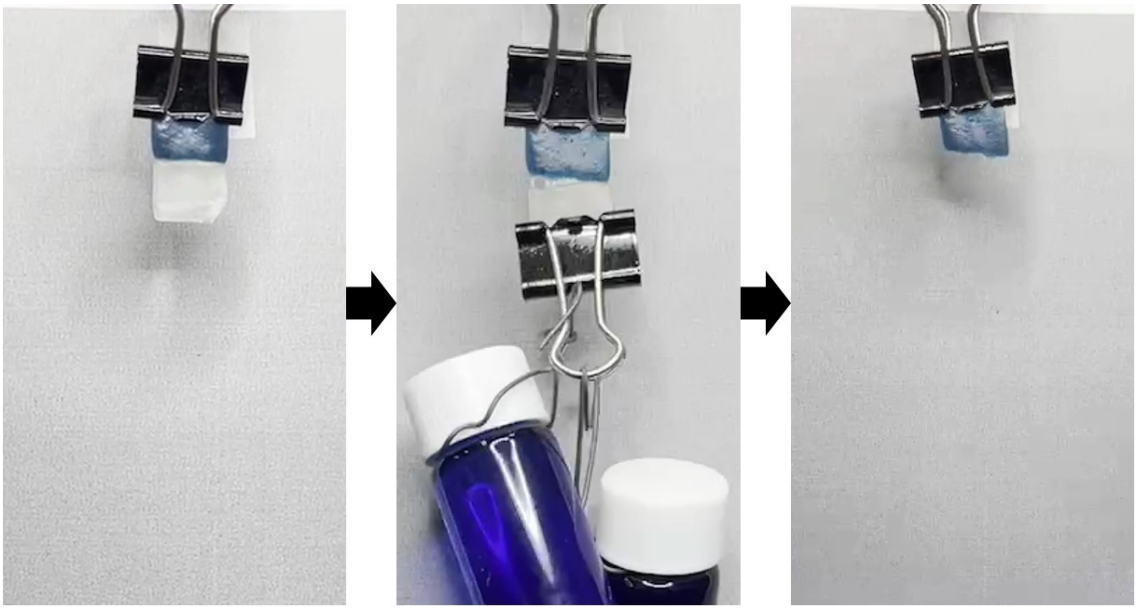

Fig. S15 Photographs demonstrating the fracture of the self-healed PIC-80 upon hanging the weight of 50 g.

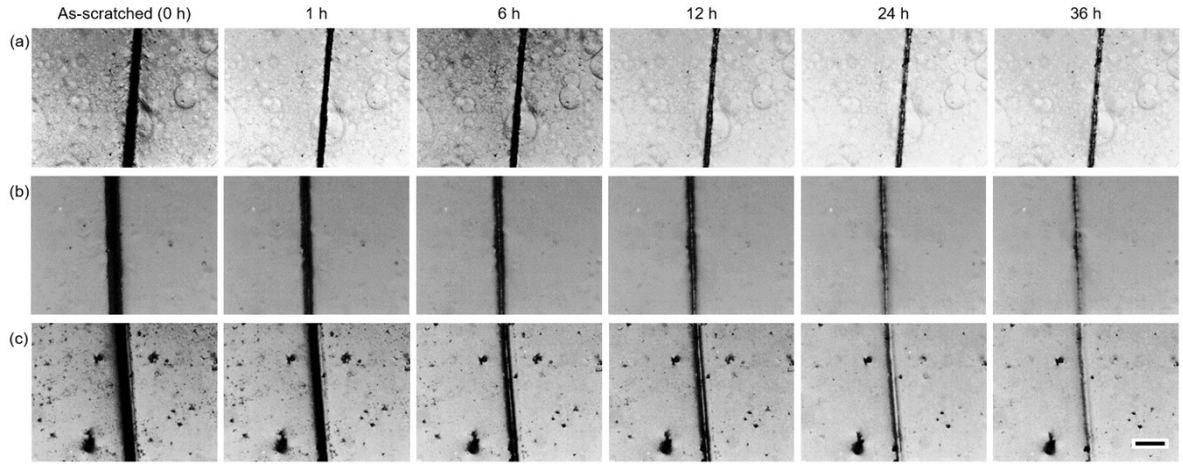

Fig. S16 Optical microscope images of scratched (a) PIC-80, (b) PIC-90, and (c) PIC-95 monitored over time (0–36 h) at RT. The scale bar corresponds to 100 μm.

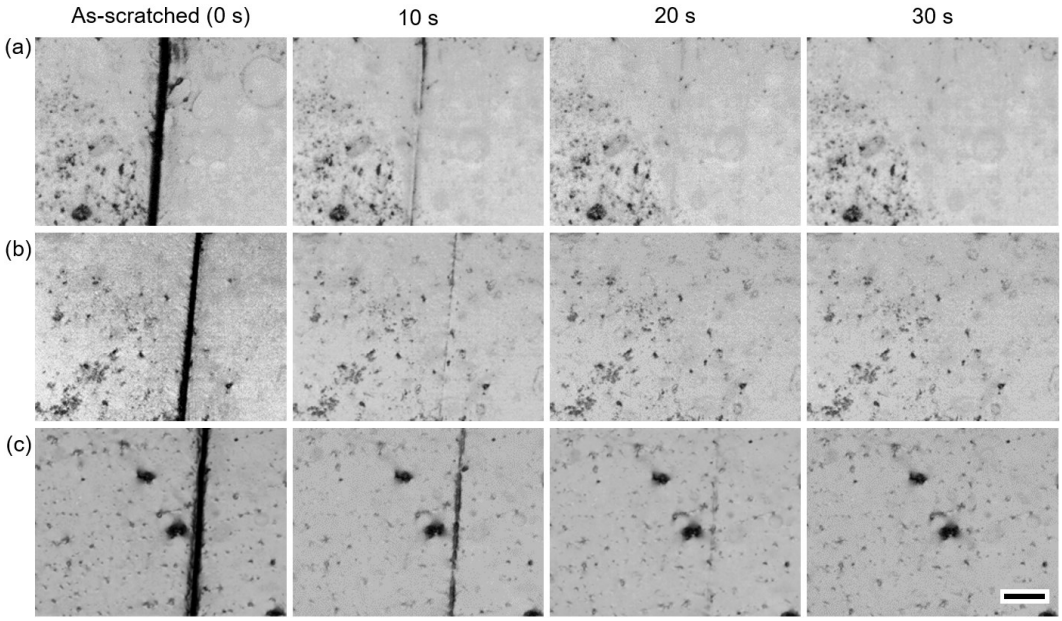

Fig. S17 Optical microscope images of scratched (a) PIC-80, (b) PIC-90, and (c) PIC-95. The scars disappeared after 30 s at 65 ˚C. The scale bar corresponds to 100 μm.

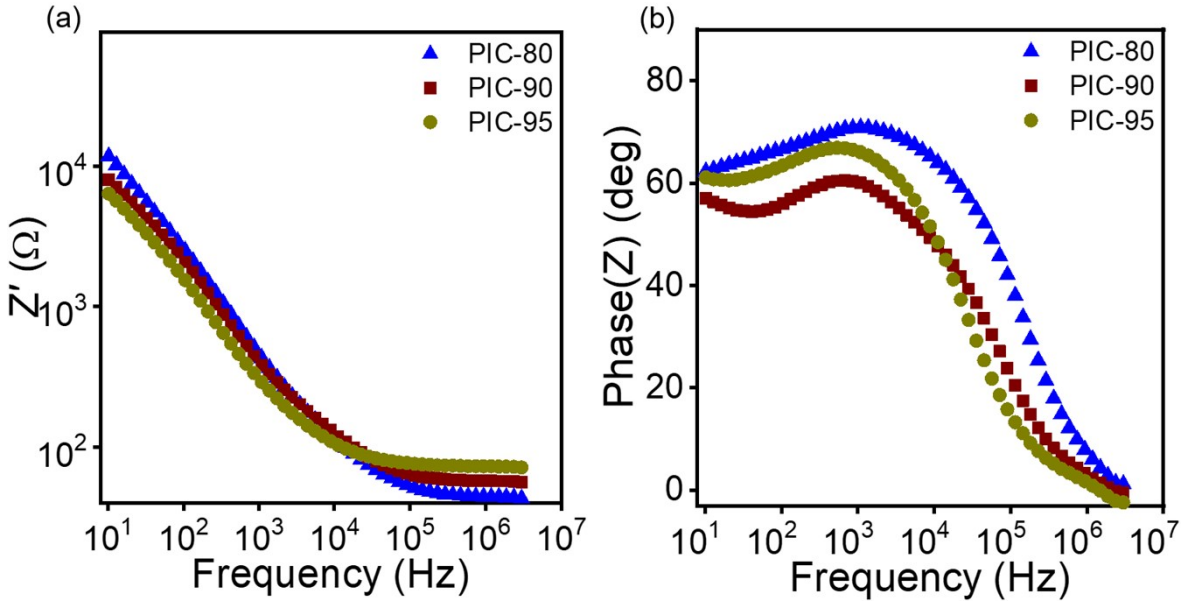

Fig. S18 (a) Z′ versus frequency graph and (b) Phase Z versus frequency graph of the PICs.

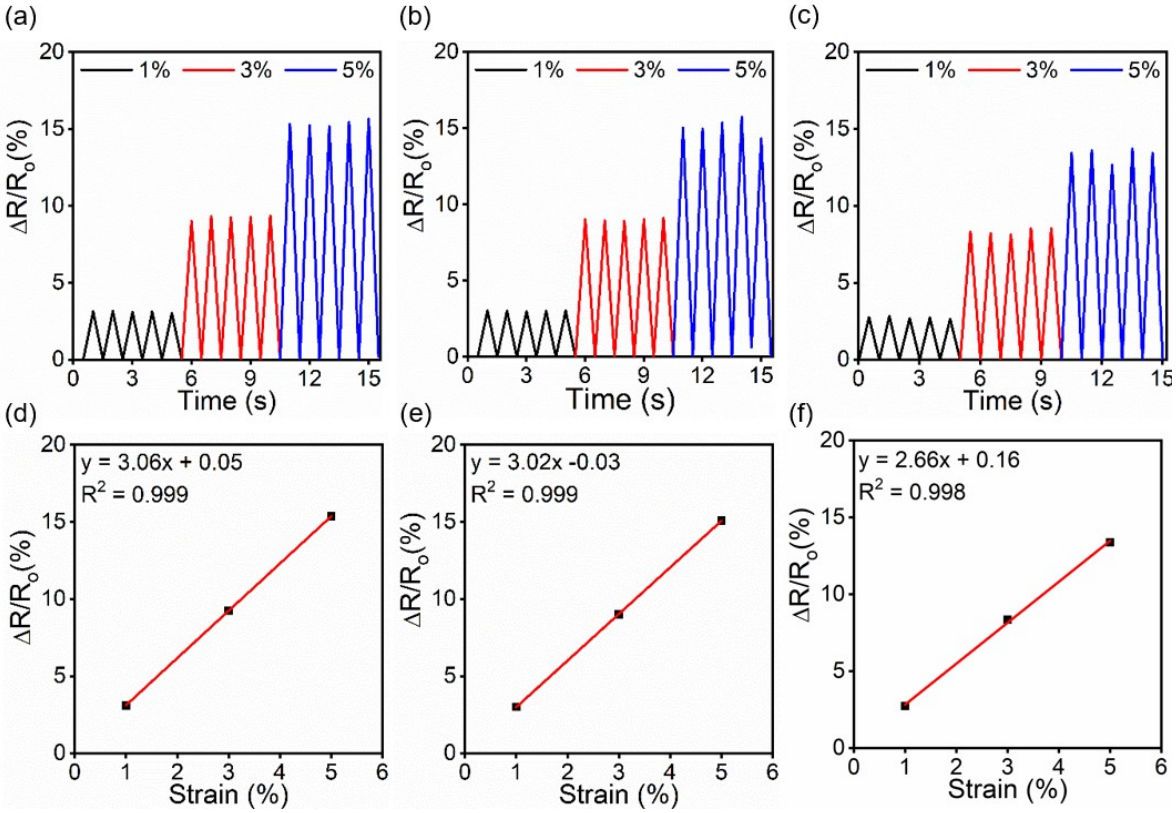

Fig. S19 $\Delta R/R_0$ as a function of the imposed strains for (a) PIC-80, (b) PIC-90, and (c) PIC-95. Linear relationships between $\Delta R/R_0$ and the tensile strains were observed for (d) PIC-80, (e) PIC-90, and (f) PIC-95.

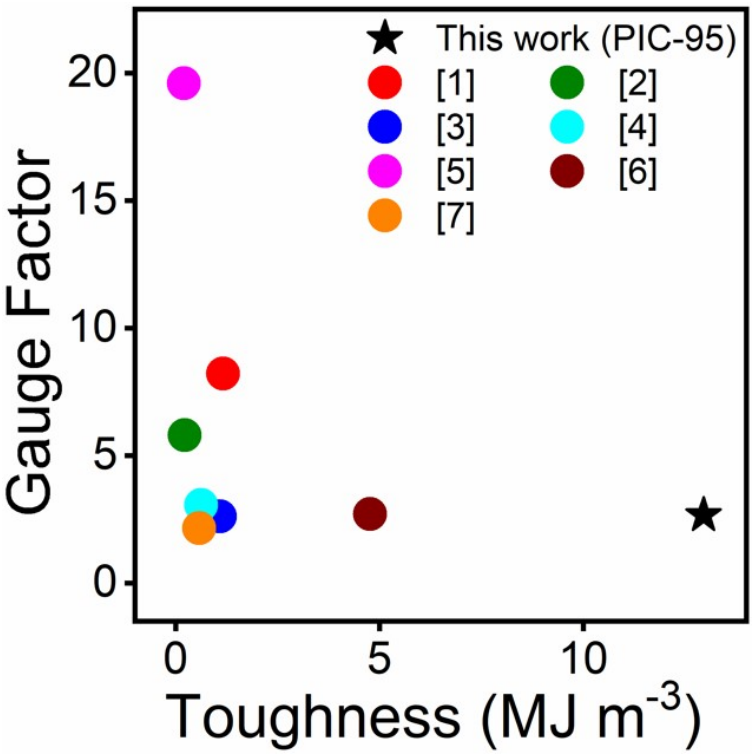

Fig. S20 Comparison between this work (PIC-95) and previous studies on gel-based strain sensors. PIC-95 is designated by an asterisk (black).

[1]Y. Wei, L. Xiang, H. Ou, F. Li, Y. Zhang, Y. Qian, L. Hao, J. Diao, M. Zhang, P. Zhu, Y. Liu, Y. Kuang and G. Chen, *Adv. Funct. Mater.*, 2020, **30**, 1804651.

[2]P. Wang, D. Pei, Z. Wang, M. Li, X. Ma, J. You and C. Li, *Chem. Eng. J.*, 2020, **398**.125540

[3]Y. Lu, X. Qu, S. Wang, Y. Zhao, Y. Ren, W. Zhao, Q. Wang, C. Sun, W. Wang and X. Dong, *Nano Res.*, 2022, **15**, 4421-4430.

[4]L. Sun, H. Huang, Q. Ding, Y. Guo, W. Sun, Z. Wu, M. Qin, Q. Guan and Z. You, *Adv. Fiber Mater.*, 2022, **4**, 98-107.

[5]L. M. Zhang, Y. He, S. Cheng, H. Sheng, K. Dai, W. J. Zheng, M. X. Wang, Z. S. Chen, Y. M. Chen and Z. Suo, *Small*, 2019, **15**, 1804651.

[6]X. Zhang, N. Sheng, L. Wang, Y. Tan, C. Liu, Y. Xia, Z. Nie and K. Sui, *Mater. Horiz.*, 2019, **6**, 326-333.

[7] D. H. Cho, K. G. Cho, S. An, M. S. Kim, H. W. Oh, J. Yeo, W. C. Yoo, K. Hong, M. Kim and K. H. Lee, *Energy Storage Mater.*, 2022, **45**, 323-331.

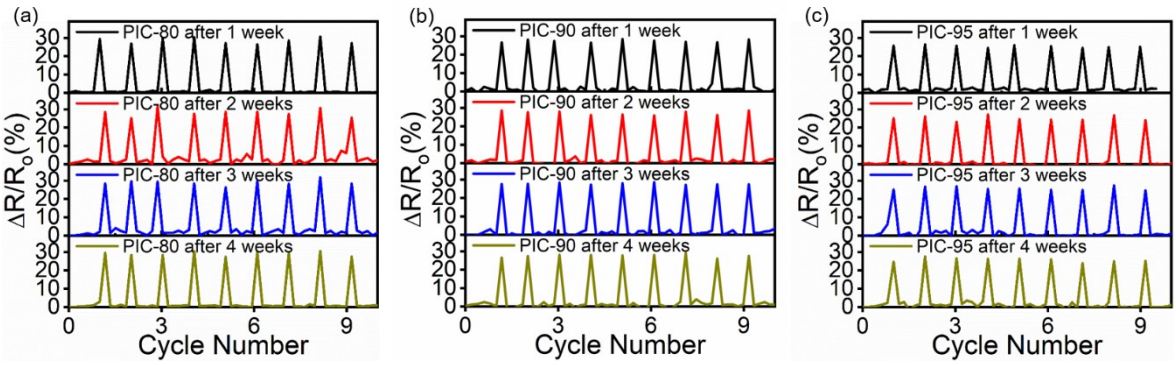

Fig. S21 Operations of (a) PIC-80, (b) PIC-90, and (c) PIC-95 strain sensors monitored over 4 weeks.

Table S1 Mechanical Properties of Polymer-IL Composites

	E (MPa)[a]	σ (MPa)[b]	ε_B (%)[c]	Toughness (MJ m^{-3})[d]	$\eta_{RT\ 6h}$ (%)[e]	$\eta_{RT\ 24h}$ (%)[f]	$\eta_{65°C\ 2h}$ (%)[g]
PIC-80	8.9 ± 0.9	0.89 ± 0.04	1300 ± 160	10.89 ± 1.10	5.3 ± 4.4	24.7 ± 5.8	108.0 ± 9.5
PIC-90	5.9 ± 0.6	0.63 ± 0.05	2100 ± 51	12.13 ± 0.86	6.9 ± 3.3	39.2 ± 1.9	105.1 ± 6.6
PIC-95	5.1 ± 0.8	0.67 ± 0.05	2400 ± 220	12.95 ± 1.02	12 ± 5.3	74.8 ± 4.6	105.8 ± 9.3

[a]Young's modulus, [b]tensile strength, [c]elongation at break, and [d]toughness of PICs. The toughness of the PICs was calculated based on the area under the stress-strain curves. The self-healing efficiencies of the composites self-healed at room temperature for [e]6 h, [f]24 h and at [g]65 °C for 2 h were estimated by the toughness of the self-healed sample with regards to the pristine samples. These results are obtained by averaging over 2–4 specimens.

Table S2 Ionic Conductivities and Gauge Factors of Polymer-IL Composites

	Ionic Conductivity (mS cm^{-1})[a]	**Gauge Factor[b]**
PIC-80	0.56 ± 0.01	3.06
PIC-90	0.40 ± 0.02	3.02
PIC-95	0.35 ± 0.01	2.66

[a]The ionic conductivities of PICs. The ionic conductivities were averaged over 2–3 measurements. [b]Gauge factors of PICs strain sensors.

Table S3 Comparison of PIC-95 to previously reported strain sensors based on autonomous self-healable gels.

Reference	Solvent	Toughness (MJ m^{-3})[a]	Self-Healing (Temperature – Time – Efficiency)	Ionic Conductivity (mS cm^{-1})	Gauge Factor	Polymer Blend
This work (PIC-95)	[EMI][TFSI]	12.95	RT – 24 h – 75%[b]	0.35	2.66	Y
[1]	Glycerol/Water	1.16	RT – 3 h – 80%[c]	1.90	4.15 – 8.21	Y
[2]	KCl/Water	0.23	RT – 30 min – 90%[c]	0.25	1.7 – 5.8	Y
[3]	[EMI][$EtSO_4$]	1.09	RT – 12 h – 90.6%[c]	-	1.04 – 2.61	Y
[4]	[EMI][DCA]	0.63	RT – 24h – 80%[c]	0.62	1.62 – 3.06	N
[5]	[EMI][$EtSO_4$]	0.20	RT – 12h – 98.7%[c]	1.00	3.82 – 19.6	N
[6]	NaCl/Water	4.77	RT – instantly – 100%[c]	0.57	2.0 – 2.7	Y
[7]	[EMI][TFSI]	0.58	RT – 1h – 100%[c]	1.75	2.14	Y

[a]Toughness was calculated based on the area under the stress–strain curves. The self-healing efficiency was estimated based on the [b]toughness and [c]elongation at break. '-' indicates 'not shown' in the reference.

[1]Y. Wei, L. Xiang, H. Ou, F. Li, Y. Zhang, Y. Qian, L. Hao, J. Diao, M. Zhang, P. Zhu, Y. Liu, Y. Kuang and G. Chen, *Adv. Funct. Mater.*, 2020, **30**, 1804651.

[2]P. Wang, D. Pei, Z. Wang, M. Li, X. Ma, J. You and C. Li, *Chem. Eng. J.*, 2020, **398**.125540

[3]Y. Lu, X. Qu, S. Wang, Y. Zhao, Y. Ren, W. Zhao, Q. Wang, C. Sun, W. Wang and X. Dong, *Nano Res.*, 2022, **15**, 4421-4430.

[4]L. Sun, H. Huang, Q. Ding, Y. Guo, W. Sun, Z. Wu, M. Qin, Q. Guan and Z. You, *Adv. Fiber Mater.*, 2022, **4**, 98-107.

[5]L. M. Zhang, Y. He, S. Cheng, H. Sheng, K. Dai, W. J. Zheng, M. X. Wang, Z. S. Chen, Y. M. Chen and Z. Suo, *Small*, 2019, **15**, 1804651.

[6]X. Zhang, N. Sheng, L. Wang, Y. Tan, C. Liu, Y. Xia, Z. Nie and K. Sui, *Mater. Horiz.*, 2019, **6**, 326-333.

[7] D. H. Cho, K. G. Cho, S. An, M. S. Kim, H. W. Oh, J. Yeo, W. C. Yoo, K. Hong, M. Kim and K.

H. Lee, *Energy Storage Mater.*, 2022, **45**, 323-331.